

SparrowSNN: A Hardware/software Co-design for Energy Efficient ECG Classification

ZHANGLU YAN* and ZHENYU BAI*[†], School of Computing, National University of Singapore, Singapore
 TULIKA MITRA, National University of Singapore, Singapore
 WENG-FAI WONG, National University of Singapore, Singapore

Heart disease is one of the leading causes of death worldwide. Given its high risk and often asymptomatic nature, real-time continuous monitoring is essential. Unlike traditional artificial neural networks (ANNs), spiking neural networks (SNNs) are well-known for their energy efficiency, making them ideal for wearable devices and energy-constrained edge computing platforms. However, current energy measurement of SNN implementations for detecting heart diseases typically rely on empirical values, often overlooking hardware overhead. Additionally, the integer and fire activations in SNNs require multiple memory accesses and repeated computations, which can further compromise energy efficiency. In this paper, we propose sparrowSNN, a redesign of the standard SNN workflow from a hardware perspective, and present a dedicated ASIC design for SNNs, optimized for ultra-low power wearable devices used in heartbeat classification. Using the MIT-BIH dataset, our SNN achieves a state-of-the-art accuracy of 98.29% for SNNs, with energy consumption of 31.39 nJ per inference and power usage of 6.1μW, making sparrowSNN the highest accuracy with the lowest energy use among comparable systems. We also compare the energy-to-accuracy trade-offs between SNNs and quantized ANNs, offering recommendations on insights on how best to use SNNs.

CCS Concepts: • **Computer systems organization** → **Embedded systems**; *Redundancy*; Robotics; • **Networks** → Network reliability.

Additional Key Words and Phrases: Energy efficient, ECG classification, Spiking neural network

ACM Reference Format:

Zhanglu Yan, Zhenyu Bai, Tulika Mitra, and Weng-Fai Wong. 2018. SparrowSNN: A Hardware/software Co-design for Energy Efficient ECG Classification. *Proc. ACM Interact. Mob. Wearable Ubiquitous Technol.* 37, 4, Article 111 (August 2018), 22 pages. <https://doi.org/XXXXXXX.XXXXXXX>

1 INTRODUCTION

Heart disease is a major cause of death among various racial and ethnic groups, with someone dying from cardiovascular issues every 33 seconds. Each year, about 805,000 Americans suffer a heart attack, and one-fifth of these are silent—causing damage without the person’s knowledge [2]. This high risk and often unnoticed damage highlight the need for continuous monitoring. Currently, monitoring has been confined to clinical

*Both authors contributed equally to this research.

[†]Corresponding author.

Authors’ addresses: Zhanglu Yan, e0385109@u.nus.edu; Zhenyu Bai, zhenyu.bai@nus.edu.sg, School of Computing, National University of Singapore, 13, Computing Dr, 117417, Singapore, Singapore, Singapore, 43017-6221; Tulika Mitra, National University of Singapore, 13, Computing Dr, 117417, Singapore, Singapore, tulika@comp.nus.edu.sg; Weng-Fai Wong, National University of Singapore, 13, Computing Dr, 117417, Singapore, Singapore, wongwf@nus.edu.sg.

Permission to make digital or hard copies of all or part of this work for personal or classroom use is granted without fee provided that copies are not made or distributed for profit or commercial advantage and that copies bear this notice and the full citation on the first page. Copyrights for components of this work owned by others than the author(s) must be honored. Abstracting with credit is permitted. To copy otherwise, or republish, or post on servers or to redistribute to lists, requires prior specific permission and/or a fee. Request permissions from permissions@acm.org.

© 2018 Copyright held by the owner/author(s). Publication rights licensed to ACM.

2474-9567/2018/8-ART111 \$15.00

<https://doi.org/XXXXXXX.XXXXXXX>

settings, using large, non-portable equipment. However, the pressing need for real-time disease detection and monitoring underscores the importance of more practical solutions. Wearable devices, therefore, emerge as a vital tool for daily continuous monitoring, offering a blend of convenience and constant health oversight [35]. Raw data from wearable devices is usually transmitted to cloud infrastructure for processing [28, 34]. However, this data offloading can consume energy, which reduces battery life and introduces delays that may hinder real-time processing [3, 35]. To address these issues, edge computing has gained traction. In edge computing, data is processed on the device itself, and only the results are sent to the cloud [12, 23]. This approach reduces energy consumption and latency, but also underscores the need for energy-efficient computing in edge applications [23].

State-of-the-art works for heart diseases are mainly focused on detection accuracy instead of energy consumption. For example, complex artificial neural networks (ANN) including attention-based temporal convolutional network (TCN) [51], convolutional neural networks [4, 40] and large language model (GPT) [24] are used for *electrocardiogram* (ECG) classification on the famous MIT-BIH arrhythmia database. Other traditional signal preprocessing methods, including random forest (RF) and voted perceptron (VP) classifiers, generally yield lower detection accuracy [42].

Unlike *artificial neural networks* (ANNs) which are known for their high energy consumption, *spiking neural networks* (SNNs) are recognized for their extremely low energy use, particularly useful for devices with limited resources like those used in edge computing [25]. SNNs differ from ANNs by transmitting binary spike trains that contain only 1s or 0s, which represent the presence or absence of a spike at each time step over a *time window* size of T . This binary mode of operation not only introduces data sparsity but also allows SNNs to perform additions in place of multiplications. For instance, computation involves only adding weights corresponding to incoming spikes, while ignoring the rest [49]. Additionally, this binary approach helps to minimize the use of complex multiply-and-accumulate (MAC) operations and reduces the required on-chip memory for storing intermediate layer activations [5, 8, 39].

However, the energy efficiency of SNNs is typically calculated based on the number of FLOPS from additions/multiplications, spike sparsity, time window size, and parameters like the product of AC energy, time window size, and sparsity rate. Unfortunately, hardware overheads such as SRAM read/write energy, scheduling, and data communications are often overlooked, even though they constitute a significant portion of total energy consumption. Furthermore, *leakage energy* (also known as static energy), which depends on the number of parameters and the number of cycles the circuit is left on, is also frequently ignored. These oversights may make SNNs appear more energy-efficient than they really are. Simple calculations based on the number of operations permit larger time window sizes, which misleadingly suggest greater energy efficiency. For instance, studies by Yan [47] and Feng [19] have adapted time window sizes of 150 and 1000 respectively for SNN inference. Although [8] highlighted the challenge of accurately estimating the energy consumption of SNNs, the issue remains unresolved, and the discussion was confined to two specific architectural examples: one employing a systolic array and the other utilizing processing-in-memory with ReRAM. Neither architecture is suitable for our application; the systolic array exceeds our ultra-low power requirements by providing excessive computational capacity, and the processing-in-memory approach with ReRAM is still too nascent to be viable for realistic applications.

Although a few ASIC-based SNN designs for ECG do account for part of the energy consumption mentioned earlier, most related works typically employ the *integrate-and-fire* (IF) or the *leaky integrate-and-fire* (LIF) model [13]. The major challenge in implementing SNNs on hardware lies in their data-driven activation functions. Both the IF and LIF models require repeated memory reads and computations across multiple time steps, with the LIF model incurring even greater hardware overhead due to the simulation of leakage actions. Unlike ANNs, which perform computations once per input, SNNs must manage a low time window size and high sparsity to achieve comparable energy efficiency and truly save energy. For instance, one SNN accelerator study suggests reducing

the time window size to just four to achieve same energy efficiency than corresponding quantized ANNs with ReRAM [31].

In this paper, we introduce a hardware-friendly spike activation mechanism named Sum-Spikes-Fire (SSF), which addresses the limitations of temporal dependency by decoupling memory access from firing models. Additionally, we co-design a network structure, SparrowSNN, which operates efficiently with a small time window size. This design not only achieves state-of-the-art accuracy for SNNs on the MIT-BIH dataset but also reduces both timestep and energy consumption. We present a complete ASIC implementation with a comprehensive analysis of the decisions of memory and computation architecture design. During the ASIC design process, we reconsidered several critical issues commonly overlooked in other ultra-low power SNN research on wearable devices. We reevaluated the workflow of SNNs, discussing and contrasting several points.

- (1) **Is the IF model effective?** We examined whether the IF model benefits accuracy and energy efficiency, and how replacing it with our Sum-Spikes-then-Fire (SSF) model could enhance accuracy, reduce memory access, and improve core computing.
- (2) **The choice between spiking CNNs and spiking MLPs:** Which is better for small SNN architectures in ECG classification?
- (3) **Can the sparsity in SNN with SSF be efficiently leveraged?** How do hardware overheads affect its performance?
- (4) **Energy Efficiency of SNNs vs. Quantized ANNs:** Is an SNN using either the IF model or our SSF model truly more energy-efficient than quantized ANNs? In which situations should quantized ANNs be preferred, considering the length of the time window size and sparsity?

During the ASIC design process, we systematically addressed each question, optimizing and evaluating energy efficiency and accuracy using the widely recognized MIT-BIH dataset. After quantizing the weights and bias to 8-bits, we can achieve an SOTA SNN accuracy of 98.29% with the energy of 31.39nJ per inference on MIT-BIH dataset. The power of our ASIC design is $6.1\mu\text{W}$. The main contributions are shown as follows:

- Rethinking SNN architecture for wearable devices from a hardware perspective, providing a detailed discussion of the disadvantages and advantages of each SNN component.
- A combined software/hardware co-design of SNN activations and networks and its ASIC implementation, achieving state-of-the-art SNN performance for ECG classification on the MIT-BIH dataset at a fraction of the energy cost.

2 BACKGROUND

2.1 Spiking neural network

Spiking neural networks (SNNs) transmit information using binary spike trains over a time window size of T , consisting solely of 0s and 1s. Utilizing rate encoding, SNNs convey membrane potential information through the firing rate of neurons, providing robust data representation [9, 37]. For instance, a value of $\frac{1}{2}$ results in a patterned spike train ($T = 4$) alternating between 0 and 1, such as [0, 1, 0, 1], effectively encoding fractional values into binary sequences. Commonly, SNNs employ the integrate-and-fire (IF) or the leaky integrate-and-fire (LIF) models as activation functions to generate these spike trains [18, 21, 36, 44]. In these models, spike generation is controlled by a voltage threshold θ . Using the LIF model as an example: at each timestep t , neuron i calculates the weighted sum of incoming spikes from the previous layer $s^{l-1}(t)$ and the corresponding weights w^l and bias b^l , adding this to the decayed previous membrane potential $\beta V_i(t-1)$ to simulate leakage. This results in the membrane potential $V_i(t)$. If $V_i(t)$ surpasses the threshold θ_i , the neuron emits a spike ($s_j^l(t) = 1$) and reduces $V_i(t)$ by θ_i ; otherwise, it outputs '0'.

$$V_i^l(t) = \beta V_i^l(t-1) + s_j^{l-1}(t)w^l + b^l \quad (1)$$

$$s_i^l(t) = \begin{cases} 1, & V_i^l(t) \geq \theta \\ 0, & \text{otherwise} \end{cases}; \quad (2)$$

$$V_i^l(t) = \begin{cases} V_i^l(t) - \theta, & V_i^l(t) > \theta \\ V_i^l(t), & \text{otherwise} \end{cases}. \quad (3)$$

For the IF model, it functions similarly to an LIF model with $\beta = 1$. Further, instead of using floating-point numbers $x_{\text{input}} \in [0, 1]$ directly for the input layer, SNN employs an encoding layer that transforms x_{input} into a spike train s_{input} over a time window of T . Previous studies have encoded spike trains using Poisson or Bernoulli distributions [17, 36], while others have implemented an integrate-and-fire approach, repeatedly applying an input $x_{\text{input}} \in [0, 1]$ to a spiking layer with a threshold of 1.0 across T timesteps to generate the input spike train [48]. In this paper, we opt for the latter method to minimize the randomness and potential sampling errors that could degrade accuracy.

Unlike traditional neural networks, the binary nature of SNNs makes them more hardware-friendly and energy-efficient [49]. However, the binary spike-based data transmission between layers prevents the use of traditional backpropagation algorithms, which rely on partial derivatives and the chain rule. To address the non-differentiability issue, two main approaches are used: SNN-specific training algorithms [38, 45] and ANN-to-SNN conversion [49]. While the former, often based on spike-timing-dependent plasticity (STDP) [41], tends to restrict networks to simpler datasets and may lead to overfitting, the latter—adopted in this study—starts with training a CNN and then transferring its weights to an SNN. This conversion approach leverages advanced CNN models and training techniques. However, directly copying weights from ANNs to SNNs can significantly reduce accuracy. To mitigate this, we employ a series of clamp and quantize (CQ) functions during ANN training, as detailed in Equation 4, to better align ANN activations with those of the SNN model [49].

$$CQ(x) = \begin{cases} 0, & x < 0 \\ \frac{\lfloor x \cdot T \rfloor}{T}, & 0 \leq x \leq 1 \\ 1, & x > 1. \end{cases} \quad (4)$$

This approach minimizes accuracy drop between the ANN-to-SNN conversion. In this study, we first train ANNs using the clamp and quantize (CQ) activation function instead of ReLU, then convert these trained ANNs into SNNs for inference. The detailed workflow is shown in Section 3.4.

2.2 MIT-BIH Arrhythmia Database

Electrocardiography (ECG) is a widely used tool for diagnosing heart diseases, providing insights into the electrical activities of the heart during each heartbeat [22]. Recently, the advent of wearable devices has made it more convenient to obtain ECG signals through built-in sensors [7, 43]. An ECG signal primarily consists of three parts: the P wave, the QRS complex, and the T wave. The P wave indicates atrial depolarization, while the QRS complex, the most prominent part of an ECG, represents ventricular depolarization [47]. The T wave is associated with the repolarization phase of the action potentials [16]. The Association for the Advancement of Medical Instrumentation (AAMI) classifies heartbeats into four major categories: normal (N), supraventricular ectopic beat (SVEB), ventricular ectopic beat (VEB), and fusion (F) as established in 1998 [20]. In this paper, we utilize the Massachusetts Institute of Technology-Beth Israel Hospital (MIT-BIH) Arrhythmia Database [32], and we align the symbols used in this dataset with the more commonly recognized AAMI classes, as shown in Table 1.

Table 1. Classes recommended by AAMI and their corresponding symbols and MIT-BIH classes.

AAMI Classes	Symbol	MIT-BIH Classes
Normal	N	N, L, R
Supraventricular Ectopic Beat	SVEB	e, j, A, a, J, S
Ventricular Ectopic Beat	VEB	V, E
Fusion	F	F
Unknown Beat	Q	/, f, Q

This dataset comprises forty-eight 30-minute ECG records from two channels, digitized at 360 samples per second per channel with an 11-bit resolution across a 10 mV range. Each record features a consistent first channel using the modified-lead II (MLII) and a second channel from one of the unipolar chest leads V1, V2, V4, or V5, varying by record. Given that MLII is present in all records and previous research by Chazal [15] demonstrated that a single lead could yield high diagnostic accuracy, we exclusively utilize MLII data in this study. The MIT-BIH dataset encompasses approximately 110,000 heartbeats, each annotated independently by two or more expert cardiologists, with any discrepancies resolved through consensus.

3 METHODS

3.1 Sum-Spikes-Fire model vs Integrate-and-Fire model

One key drawback of the IF/LIF model is its requirement to access memory and perform computations T times due to the data dependency between different time steps. However, with rate-encoded spike trains used to represent information between layers, the crucial factor is the total number of spikes, not the sequence or timing of these spikes. In Sum-Spikes-Fire model, we first calculate the total number of spikes and then compute the weighted sum of these spikes against the weights to determine the accumulated membrane potential. This sum is compared to $T\theta$ to generate the spike train for the next layer, shown in Algorithm 1. Notably, memory needs to be accessed only once to compute the membrane potential.

Moreover, when the time window size is small, particularly for T values less than 16, the Sum-Spikes-Fire (SSF) model enhances the robustness and performance of SNN models. This improvement addresses a common issue in IF/LIF models, where potential accumulation tends to squeeze into the final timesteps. For instance, if the membrane potential at the last timestep is double the threshold θ , only one spike is generated instead of two due to the binary nature of spike trains. This squeezing effect can prevent firing models from spiking in time, leading to information loss due to residual membrane potential. Conversely, SSF models address this by generating spike trains based on the sum of membrane potentials, thus incorporating global information and mitigating loss.

Furthermore, by only requiring a count of spikes, we can decrease the memory access cost from T to $\log_2(T+1)$. The SSF mechanism also leads to a more efficient hardware implementation for both memory and computing components. The energy consumption analysis later in Section 5.3.2 shows the better energy efficiency of SSF compared to the IF model where the membrane potential is accumulated multiple times.

3.2 Network design

The design of the network should consider three main factors: 1) the number of parameters, which determines the size of the memories and the amount of memory access to load them into the compute units; 2) the core computing energy, which varies across different inference modules; 3) the intermediate output storage, which also contributes to energy consumption of memory systems.

We analyze two prevalent network architectures for ECG classification: the spiking convolutional neural network (SCNN) and the spiking fully connected network (SMLP). The energy consumption of SCNN is determined

Algorithm 1 Sum-Spikes-Fire (SSF) models.

Require: Time window size of T ; Weights w^l and bias b^l at layer l ; Input spike train s^l at layer l ; Membrane potential v_t^l of at layer l at time step t . Default threshold θ .

```

1: STEP1: Sum-spikes
2:  $S^l = 0$ 
3: for  $t = 1$  to  $T$  do
4:    $S^l += \sum w^l s_t^l + b^l$ 
5: end for
6: STEP2: Fire
7:  $V^l(0) = 0$ ;
8: for  $i = 0$  to  $T - 1$  do
9:    $V^l = V^l + S^l$ 
10:  if  $V^l \geq T * \theta$  then
11:     $s_i^{l+1} = 1$ 
12:     $V^l = V^l - T * \theta$ 
13:  else
14:     $s_i^{l+1} = 0$ 
15:  end if
16: end for

```

by the number of input/output channels (c_i/c_o), the size of 1-D input/output signals (x_i/x_o), and the kernel size (k). For SMLP, energy depends on the input/output dimensions (d_i/d_o) and the time window size (T). All weights and biases are quantized to 8 bits, and our SNN operates with a time window size of 8. We detail the energy for parts 1, 2, and 3, based on the energy per memory access ($E_{m,1}, E_{m,3}$) and per computation (E_c):

$$E_{SCNN} = (c_i \cdot c_o \cdot k + c_o) \cdot E_{m,1} + (c_i \cdot c_o \cdot k \cdot x_o + c_o \cdot x_o) \cdot E_c + 2 \cdot c_o \cdot x_o \cdot T/8 \cdot E_{m,3} \quad (5)$$

$$E_{SMLP} = (d_i \cdot d_o + d_o) \cdot E_{m,1} + (d_i \cdot d_o + d_o) \cdot E_c + 2 \cdot d_o \cdot T/8 \cdot E_{m,3} \quad (6)$$

While convolutional methods generally require more core computing than fully connected networks, they have fewer parameters to store. However, convolutional networks produce larger intermediate outputs, necessitating more memory than fully connected networks. To match the SMLP accuracy, a typical SCNN setup needs a kernel size (k) of 9 and channel numbers (c_i/o) of 18, compared to an SMLP with an output dimension (d_o) of 64 per layer. Given an ECG input size (s_i) of 180, the energy costs are $17388E_m + 428490E_c$ for a 3-layer SCNN with the hyperparameters mentioned above and $16856E_m + 16520E_c$ for 3-layer SMLP with hyperparameters mentioned above. In our ultra-low-power ASIC design, there is a single memory level directly connected to the compute core, eliminating the need for a hierarchical memory structure; thus, the energy costs for the first and third memory levels ($E_{m,1}$ and $E_{m,3}$) are comparable and collectively referred to as E_m . Then, we can address question 2) from the introduction: Given that SCNNs require large input/output channels and kernel sizes to achieve comparable accuracy, which in turn increases the core computing energy, we have chosen to focus on MLP-type SNNs in this study. The network structure is presented as follows:

3.3 Post-training Static Quantization for SNN

We enhance energy efficiency in SNNs by quantizing weights and biases to 8 bits. We determine the joint maximum and minimum values of the weights and biases for each layer, calculate a rescaling factor r , and map

Table 2. SMLP Network structure.

	Input dimension	Output dimension	Number of parameters	Activation function
Layer1	180	56	10136	SSF
Layer2	56	56	3192	SSF
Layer3	56	56	3192	SSF
Classification layer	56	4	224	/

the weights w and biases b to 8-bit integer values w_q and b_q , respectively. For SNN inference, we adjust the threshold using the same rescaling factor, as detailed in Algorithm 2.

Algorithm 2 SNN weight/bias quantization

Require: Weight w^l of layer l ; Bias b^l of layer l ; Quantization level q that quantized weight/bias to q -bits integer; Origin threshold of this SNN layer θ .

- 1: $f_{\max} = \max\{w^l, b^l\}$
 - 2: $f_{\min} = \min\{w^l, b^l\}$
 - 3: $r = \frac{(f_{\max} - f_{\min})}{2^q - 1}$
 - 4: $w_q^l = \text{clamp}\{\lfloor (w^l/r) \rfloor, -2^{q-1}, 2^{q-1} - 1\}$
 - 5: $b_q^l = \text{clamp}\{\lfloor (b^l/r) \rfloor, -2^{q-1}, 2^{q-1} - 1\}$
 - 6: $\theta_q = \lfloor \theta/r \rfloor$
 - 7: return w_q, b_q and θ_q
-

3.4 Workflow of SparrowSNN

In this section, we outline the training and inference workflow of SparrowSNN. Initially, we train the MLP using a clamp and quantization function (see Equation 4) along with batch normalization. Subsequently, we integrate the batch normalization into the weights and biases for inference purposes. The weights and biases are then quantized, and the MLP is converted into a spiking MLP by replacing the floating inputs with spike input trains and substituting the clamp and quantization function with the SSF model for inference. The workflow is illustrated in Figure 1.

4 ULTRA-LOW POWER ASIC DESIGNS FOR SNN

Implementing Spiking Neural Network (SNN) models into ASIC designs requires a nuanced approach beyond straightforward software-to-hardware translation. Instead, a co-design strategy integrating both software and hardware is imperative to optimize system performance. This section quantitatively explores the trade-offs between performance and power consumption associated with different designs of computational and memory components in an ultra-low-power ASIC context. It aims to identify the most efficient design for our SNN model with SSF.

4.1 Dynamic and Static Power Consumption

Power consumption in silicon-based circuits can be categorized into two types: dynamic and static. Dynamic power consumption occurs during state transitions in the circuit, driven by the charging and discharging of capacitances and transient short-circuit currents in transistors. It is predominantly proportional to the operational frequency and is only incurred during changes in the circuit's state. Conversely, static power, also known as

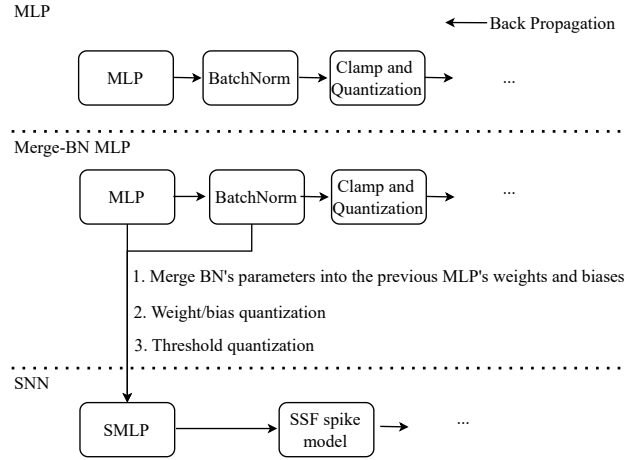


Fig. 1. Workflow of SparrowSNN

leakage power, persists regardless of state changes. In ultra-low-power systems with minimal computational demands, static power consumption becomes a significant factor and must be carefully managed.

Table 3 illustrates the power consumed by a single computational unit (the design details of our compute unit are provided later) at various operational frequencies. The dynamic power closely correlates with frequency, while static power remains relatively constant. The ratio of dynamic to static power indicates power efficiency. At frequencies below 1MHz, efficiency is low and such configurations should be avoided. Above 4MHz, dynamic power becomes dominant over static power, marking these configurations as more efficient. However, operating at higher frequencies, while generally improving efficiency, can also introduce complexities such as timing challenges and increased overhead in non-computational components like memory buses. These factors can ultimately compromise the overall energy efficiency of the system.

Frequency(Hz)	Dynamic Power (uW/%)	Static Power (uW/%)	Total Power (uW)
1G	217.653300 (99.93%)	0.143600 (0.07%)	217.796900 (100%)
100M	21.341190 (99.40%)	0.129200 (0.60%)	21.470390 (100%)
10M	2.134119 (94.29%)	0.129200 (5.71%)	2.263319 (100%)
5M	1.067057 (89.20%)	0.129200 (10.80%)	1.196257 (100%)
4M	0.853673 (86.85%)	0.129200 (13.15%)	0.982873 (100%)
2M	0.426850 (76.76%)	0.129200 (23.24%)	0.556050 (100%)
1M	0.213412 (62.29%)	0.129200 (37.71%)	0.342612 (100%)
100K	0.021341 (14.18%)	0.129200 (85.82%)	0.150541 (100%)
10K	0.002134 (1.62%)	0.129200 (98.38%)	0.131334 (100%)

Table 3. The Dynamic and static power of our reference design for different frequency

4.2 Memory Design

Memory components are crucial for storing various data elements like weights, biases, thresholds, and activation values. Given their size, it is impractical to store all these data within the computation unit using flip-flops due to

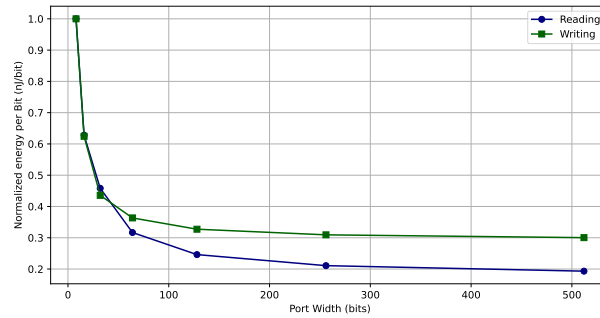


Fig. 2. Energy Consumption per bit of SRAM block for different bus width

their space and energy inefficiency. Therefore, incorporating RAM blocks outside the computation unit (CU) is essential, with data being transferred in and out of the CU as needed.

For devices that are always on and have stringent low-power requirements, Static Random Access Memory (SRAM) is the most suitable choice. SRAM's design, which primarily uses transistors, also incurs leakage power proportional to its total size. The dynamic power consumption of SRAM depends on the frequency of read and write operations and is also influenced by the bus width—the number of bits read or written per operation.

The bus width has significant implications for energy efficiency: larger bus widths improve energy efficiency per bit due to reduced overhead in accessing memory. However, they also make the design less flexible by necessitating memory operations to handle larger data chunks at once. For quantitative analysis, we synthesized SRAM blocks using a commercial 22nm SRAM IP configured for low leakage power. Figure 2 illustrates the energy consumption per bit for different memory bus widths of SRAM blocks of the same size, all normalized to a bus width of 8.

The results indicate that energy efficiency per bit improves significantly when increasing the bus width from 8 bits to 64 bits, but the gains are slower beyond 64 bits. This finding underscores the trade-off between energy efficiency and design flexibility, which must be carefully balanced, especially in low-power, Always-On applications.

4.3 Improving the energy efficiency with the SSF mechanism

One key aspect of the SSF mechanism is that the membrane potential of an output neuron does not depend on the position of the ones in the input spike train but rather on the number of ones in the input spike train. That means the T-timestep accumulation can now be represented by a $(\log_2 T - 1)$ -bit Multiply-and-Accumulation (MAC) operation. This key difference leads to better energy efficiency in computation and memory transactions.

MAC operation is more efficient than consecutive additions. From a computation aspect, a 3-bit by 8-bit multiplication effectively substitutes for a maximum of 7 consecutive additions; a 4-bit by 8-bit multiplication for 15 consecutive additions. Table 4 compares the energy consumption of MAC units to an addition-and-accumulation unit (ACC). Both are synthesized with the same commercial 22nm technology node. The size of the accumulation register is 16-bits while the input sizes are different. The MAC units have higher leakage power, while their dynamic power is not scaled linearly with respect to the size of input. This is primarily because the energy consumption is dominated by the 16-bit register involved in both operations. Moreover, using ACC leads to more

computing cycles and worse energy efficiency. Consequently, our SSF mechanism using MAC operation profits better energy efficiency in the compute unit.

	Dynamic Power	Leakage Power	Total
4b-8b-16b MAC	0.0789	0.0434	0.1223
3b-8b-16b MAC	0.0688	0.0356	0.1044
8b-16b ACC	0.0545	0.0177	0.0722

Table 4. Power consumption of MAC and ACC operations

The SSF model improves the memory efficiency. First, in the classical SNN with IF mechanism, the weights should be loaded for each timestep, resulting in redundant memory loads of weights across timesteps. In contrast, our SSF mechanism only requires the number of ones in the spike train which is encoded as an integer; the computation for all timesteps is performed at once.

Second, our SSF mechanism utilizes the memory bandwidth more efficiently. Each spike train is loaded as an integer rather than the bits across timesteps. Considering the lower efficiency of memory transfers at small bus widths as discussed in Section 4.2, the SSF mechanism also improves the memory efficiency.

As a result, our design using the SSF mechanism demonstrates superior energy efficiency, performance, and scalability in such an ultra-low-power design when compared to traditional SNN implementations using IF. Detailed experimental results and comparison can be found in Section 5.

4.4 ASIC design

Matching the Computation Capability with Requirements: The computing capability of the system can be roughly estimated by $N_{CU} \times f$, where N_{CU} is the number of computing units and f indicates the frequency. The system's design space can be explored in both temporal and spatial dimensions: using more computation units at a lower frequency or fewer computation units at a higher frequency. Considering the frequency-energy trade-off discussed in Table 3, we can determine the optimal number of computation units required by our system.

The required number of inferences for our SNN model on the ECG application should match the sampling rate if we consider a sliding window fashion process. The MIT-BIH dataset's sampling rate of 180 Hz will be used as an example in the following discussion. For the ECG application, the required number of inferences should match the sampling rate if we consider a sliding window fashion process. The MIT-BIH dataset's sampling rate is 180 Hz, which we will consider as an example in the following discussion. For our SMLP model, as we mentioned in section 3.2, the number of operations per layer can be calculated by $d_i \times d_o + d_o + N_{activation} \times d_o$. $d_i \times d_o$, where $d_i \times d_o$ represents the MAC operations required for the weighted sum (accounting for MAC as one operation), each neuron requires one addition to add the bias ($+d_o$), and one activation function ($N_{activation}$ operations per activation) is performed per output neuron.

The total computation is the sum of the computation of all layers. For our SNN model, it is $(180 \times 56 + 56 + 16 \times 56) + (56 \times 56 + 56 + 16 \times 56) \times 2 + (56 \times 4) = 20140$ operations per inference. This results in approximately 3.6 million operations per second for a target of 180 inferences per second. Even with a single computation unit at 4MHz, the dynamic power is not yet in the most efficient range (see Table 3). Thus, we conclude that a single computation unit is sufficient for our example of SNN inference for ECG applications.

Memory design for SNN ASIC design: In the design of our SNN model with SSF, the memory operations associated with different computational components exhibit unique characteristics. During the computation of the weighted sum, each pair of output and input neurons requires simultaneous access to the corresponding weights and activations; this necessitates frequent memory operations. In contrast, when computing neuron

activations, the bias is loaded once per neuron, the threshold once per layer, and the activation result is stored once per neuron. Notably, the operations involving weight and activation retrieval constitute the majority (98.6%) of memory interactions.

Furthermore, for each output neuron's weighted sum computation, the related weights and activations can be stored contiguously in memory. This arrangement allows for more efficient bulk memory operations, enhancing overall memory usage efficiency as discussed in Section 4.2. However, in our SNN model, each weight is represented as an 8-bit value and each activation as a 4-bit value when $T = 15$, and they are accessed synchronously for each MAC operation. To optimize this, we separate the storage for weights and activations. We use Static Random Access Memory (SRAM) configured as Read-Only Memory (ROM) for storing all immutable data such as weights, biases, and thresholds, with a bus width of 64 bits. For activations, which are mutable and accessed frequently during computations, we allocate a dedicated SRAM with a bus width of 32 bits. This configuration aligns the loading cycles for weights and activations, facilitating synchronized access for every eight MAC computations.

The architecture. Algorithm 3 outlines the sequence of computations for an SNN inference with SSF. As our design includes only one computation unit (CU), this CU is responsible for all computations. The required operations are: Multiply-and-Accumulate (MAC), bias addition, threshold comparison, and subtraction of the threshold from the accumulator. Different datapaths within the CU are allocated for these operations and managed by a scheduler equipped with a finite-state machine (FSM). The scheduler also orchestrates memory operations by generating appropriate addresses and controlling read/write signals to the memories, based on the FSM's current state.

Figure 4 presents the complete architecture design, and Figure 3 details the FSM functionality. One inference cycle comprises four primary steps:

- **MAC Step:** Weights and activations are fetched from the ROM and RAM, respectively. The products are accumulated in a 16-bit accumulator, with each MAC operation completed in one cycle. Given the memory bus width supports 8 MAC operations, memory is accessed every 8 cycles and buffered at the multiplier's input. The scheduler tracks the input neuron indices and transitions to the BIAS ADD step once all inputs are processed.
- **BIAS ADD Step:** Bias values are loaded from the ROM and added to the accumulator in a single cycle, followed by a transition to the ACTIVATION state.
- **ACTIVATION State:** Over 8 cycles, the accumulator's value is added to itself and compared with the threshold, updating the output buffer bit-wise for each cycle. If the accumulator exceeds the threshold, the threshold value is subtracted from it and the corresponding bit is set to 1, 0 otherwise. The scheduler monitors the output neuron index, and upon completing the current layer, triggers threshold loading into a 16-bit register.
- **SAVE Step:** The output buffer is saved back to the SRAM. The SRAM double buffers the activations to avoid overwriting the previous layer's output. Then, the FSM returns to the MAC state for the next neuron or layer. If an entire inference cycle is complete, the FSM resets to prepare for the next inference.

4.4.1 Performance. The performance of our ASIC design is perfectly predictable with respect to the FSM. We detail the number of cycles and the number of memory operations for each state of the FSM. For each layer, the total number of cycles of computation c_l is composed of the cycles on each state of the FSM.

$$c_{MAC} = d_{input} \times d_{output} \quad (7)$$

$$c_{BIAS} = c_{SAVE} = d_{output} \quad (8)$$

$$c_{activation} = 8 \times d_{output} \quad (9)$$

$$c_l = c_{MAC} + c_{BIAS} + c_{activation} \quad (10)$$

The total number of cycles per inference is 21760. Considering a frequency of 4MHz, we achieve a throughput of 221.14 inferences per second.

The memory operations can also be perfectly predicted. For each layer:

$$n_{LOAD_weights} = \lceil d_{input} \div bus_width \rceil \times d_{output} \quad (11)$$

$$n_{LOAD_bias} = n_{LOAD_activation} = n_{STORE_activation} = d_{output} \quad (12)$$

The threshold is loaded once per layer, hence $n_{LOAD_threshold} = |L|$.

The detailed experimental results of performance and energy consumption can be found in Section 5.

Algorithm 3 Computation of one SNN inference with SSF

```

1: OUTPUT_BUF[8] // output buffer
2: W[l][ni][no] // the weights, in ROM
3: THRESHOLD[l] // the thresholds, in ROM
4: BIAS[l][n] // the BIAS, in ROM
5: ACTIVATIONS[2][n] // the outputs of the neurons of the current
   layer, stored in SRAM, doubled buffered
6: for l ∈ Layers do
7:   for n ∈ Neurons[l] do
8:     for nprev ∈ prev(l) do
9:       activation := ACTIVATION[l%2][nprev]
10:      ACC := ACC + W[l][nprev][n] × activation
11:     end for
12:    ACC := ACC + BIAS[l][n]
13:    for t ∈ (0, 16) do
14:      if ACC > THRESHOLD[l] then
15:        ACC := ACC - THRESHOLD[l]
16:        OUTPUT[n%8] := OUTPUT[n%8] + 1
17:      end if
18:    end for
19:    CLEAR(ACC);
20:    SAVE(OUTPUT);
21:    CLEAR(OUTPUT);
22:  end for
23: end for

```

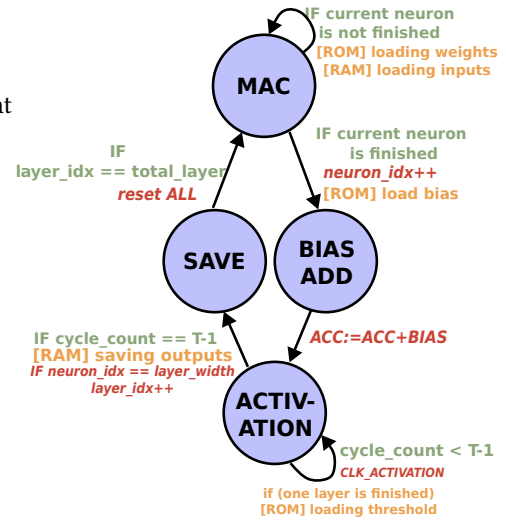


Fig. 3. The FSM. TODO: make it more vertical to save place

4.5 Handling the sparsity in SNN

This section evaluates the potential of leveraging sparsity in the activation values of SNN models, which are known to exhibit high sparsity [46]. Specifically, we explore the implications of incorporating sparsity into our ultra-low-power design. Despite the potential benefits, our findings indicate that leveraging sparsity actually leads to increased energy consumption.

In SNN models, sparsity manifests in the activation values, which are determined at runtime. To exploit this sparsity, an additional mechanism is necessary to skip the zero activations dynamically, allowing the system to bypass computations for zero values. However, since the weights are statically stored in memory and the sparsity pattern of activations is unknown until runtime, it becomes necessary to match the memory bus width with the weight size (8-bit) to read only the requisite weights for non-zero activations.

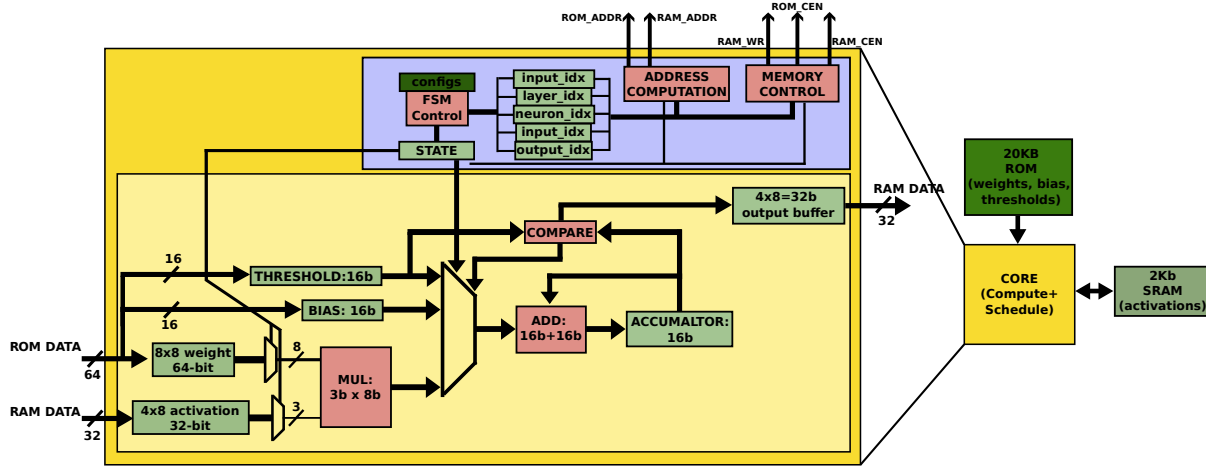


Fig. 4. The design of the CU and the scheduler associated.

For our ultra-low-power SSF design, we can add an extra step in the FSM to check the activation value before proceeding with the MAC operation. If the activation value is zero, the MAC operation is skipped. While this approach theoretically reduces the number of computations, it introduces two significant overheads in our design:

- Zero-Detection Mechanism: An additional component in the computation unit (CU) is required to detect zero activations, which adds complexity and energy consumption.
- Reduced Memory Bus Efficiency: Narrowing the memory bus width to align with the weight size decreases its efficiency. This is particularly impactful because the memory bus contributes significantly to the system's total energy consumption.

Experimental results demonstrate that with the sparsity-aware mechanism, overall energy consumption increases by 66%. This increase is primarily attributed to the inefficiencies introduced by the narrower memory bus. Given these findings, we have decided against incorporating the sparsity mechanism into our ultra-low-power design, and resolving Question 3 of the introduction.

5 RESULTS

5.1 Experiment Setup

In this study, we utilized CUDA-accelerated PyTorch version 1.12.1+cu116 for training. Experiments were conducted on a system equipped with an AMD EPYC 7763 64-Core Processor, 1000GB of DRAM, and dual NVIDIA A100 GPUs. The operating system was Linux 5.15.0-86-generic x86_64. Our ASIC design with a commercial 22nm process with FD-SOI technology. The synthesized frequency is set to 4MHz for our SNN with SSF model.

5.2 preprocessing

In this study, we use the MIT-BIH dataset for ECG classification. We excluded four of the dataset's 48 records (numbers 120, 104, 107, and 217) as recommended by AAMI [27, 30], due to significant imbalances in beat types within these records. Additionally, we removed the baseline and normalized the remaining records to the range [0, 1], following methods from prior research [15, 30]. In this dataset, the R peaks are manually annotated; thus, we extracted a window of 180 data points centered around each R peak—90 points on each side—to segment the beats.

To construct the training and inference dataset, we allocated 60% of the heartbeats for training, 20% for testing, and an additional 20% for per-patient online training to develop a patient-specific model. Given the imbalance in the training dataset, we employed synthetic minority oversampling (SMOTE) [11] to achieve a balanced dataset. We also present the class distributions before and after this data augmentation

Table 5. Training Data Extension with SMOTE.

	Original training dataset	SOMTE-augmented training dataset
Number of N	53872	53872
Number of SVEB	1817	53872
Number of VEB	4215	53872
Number of F	482	53872

We further illustrate the morphology of various heartbeat types after data processing using patient record number 200 as an example. We selected one normal (N) heartbeat, one supraventricular ectopic beat (SVEB), one ventricular ectopic beat (VEB), and one fusion (F) heartbeat for comparison, as shown in Figure 5.

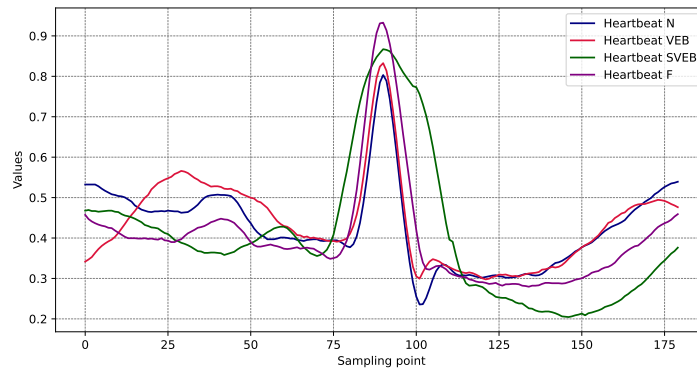


Fig. 5. N, SVEB, VEB and F heartbeats

5.3 SNN performance analysis

5.3.1 Model Accuracy. In this section, we evaluate an 8-bit quantized weight SNN across various time window sizes (T) and activation functions, including the IF and SSF models. To ensure a fair comparison, we also benchmark against an 8-bit ANN with 8-bit activations. We follow the SNN training methods described in Section 3.4. For the ANN, we utilize the same network architecture as the SNN, consisting of three MLP layers with an output dimension of 64 and a classification layer, trained using the ReLU function. We perform ANN quantization using Pytorch post train static quantization [1]. We compare the performance at time window sizes of 3, 7, 15, and 31 ($2^l - 1$), allowing us to assess the impact of T on model effectiveness. We synthesize all hardware using the same 22nm tech node.

As illustrated in Figure 6(A), the SNN with the SSF model consistently outperforms the SNN with the IF model. For instance, with $T = 3$ and 7, the SSF model achieves accuracies 15.1% and 15.42% higher than the IF model, due to its enhanced robustness. As T increases to 31, the accuracy disparity between the IF and SSF models narrows to

1.39%. Moreover, when T exceeds 15, the accuracy of the SNN with the SSF model surpasses that of the baseline 8-bit ANN.

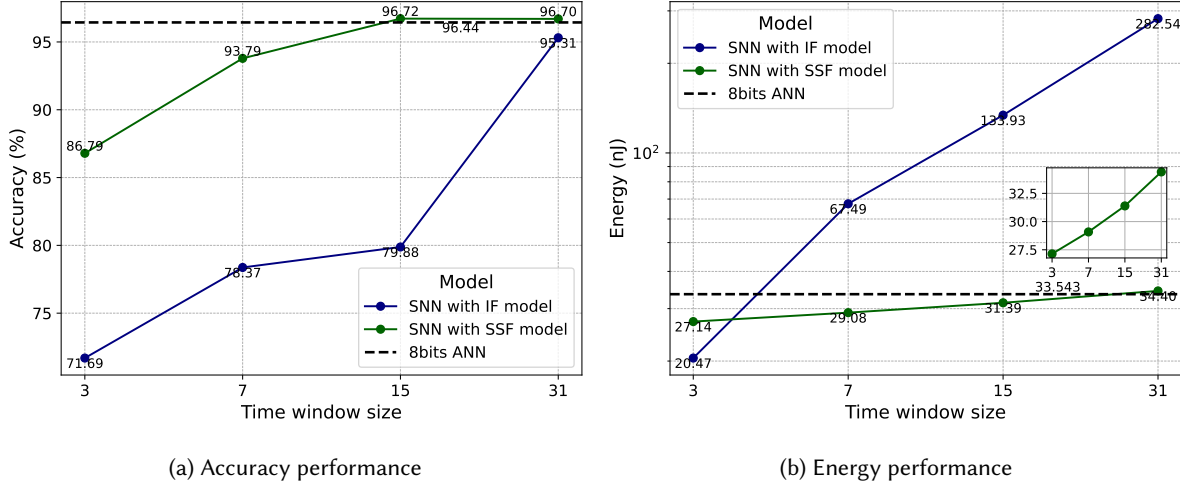


Fig. 6. SNN accuracy and energy performance comparison

5.3.2 Energy Consumption. We synthesize the core hardware previously using a commercial 22nm technology node. Table 6 reports the power consumption breakdown of the core.

Table 6. Power Consumption Analysis (power numbers in μW)

Power Group	Dynamic Power	Static Power	Total Power
register	0.803712	0.051231	0.854943
combinatorial	0.049960	0.077941	0.127901
total	0.853672	0.129172	0.982844

For the memory components of our designs, both the 20KB ROM and the 2KB SRAM were synthesized using the SRAM IP from the same commercial 22nm technology node as the core, specifically configured for low leakage power to enhance energy efficiency. This configuration aligns with our focus on ultra-low-power design principles. Table 7 reports the read and write energy and the leakage power of the memory blocks.

Table 7. The Memory Synthesis result

Memory Size	Bus Width	Read Energy(nJ)	Write Energy(nJ)	Leakage Power(μW)
20KB	64-bit	0.0075	0.0074	0.48
2Kb	32-bit	0.0030	0.0029	0.026

As we can determine the number of cycles and the number of memory reads and writes statically, we can obtain an accurate estimate of energy consumption for our system. Assuming $T = 15$, Table 8 details the energy consumption per inference (in nJ) for different operations and the proportion of each in the total energy

consumption. As shown in Table 8, the leakage power of our design is low. Our SNN model with SSF employs simple operations: one type of multiplication, one type of MAC operation, and one comparison. This allows us to integrate all these functions within a single CU, thus achieving the target throughput with a frequency in a favorable range, which minimizes the ratio of the leakage energy to only 1%. Memory operations consume the majority of the energy. However, we have already achieved optimal usage of the memory operations since each required weight or activation is loaded only once.

ROM energy	RAM energy	Mem Leakage	Core Dynamic	Core Leakage	Total leakage	Total
16.88(53.77%)	6.78(21.60%)	2.43 (7.74%)	4.58 (14.59%)	0.71 (2.26%)	3.14 (1.00%)	31.39(100%)

Table 8. Energy Consumption per inference(nJ) and their ratio

For a comprehensive comparison between different models, we also synthesize the hardware for SNN with IF and 8-bit ANN using the same technology node. These models followed the same underlying architectural principles but featured some differences tailored to their computation paradigms:

- In the ANN model, components related to threshold and activation in the SNN are replaced by those necessary for rescaling activities in ANNs.
- For the SNN with IF, the MAC unit is replaced by a simple accumulation unit, reflecting the simpler computational requirements of this model.
- The Finite State Machine (FSM) is adapted for each model to match the specific computational sequence required by their respective processing mechanisms.

These modifications ensure that each hardware iteration is optimized for its specific computational model while maintaining a consistent architectural baseline for fair energy consumption comparison. This approach allows us to directly evaluate the impact of the different computational strategies on energy efficiency and overall performance. The complete energy consumption for both the IF and SSF models is depicted in Figure 6(B). For the IF model, assuming optimal hardware management of sparsity, we adjust the energy calculation by multiplying it with the spike rate (the ratio of non-zeros bits). In summary, we can make the following observations:

- When the time window size is small, and sparsity ranges from 65% to 75%, memory access is minimized by not performing reads when the input spike is zero. Consequently, for $T < 3$, the IF model exhibits better energy efficiency than the SSF model.
- However, the accuracy at $T = 3$ is significantly lower than that of the SNN with the SSF model.
- Comparing the baseline quantized ANN to the SNN with the SSF model, we find that the SSF SNN is more energy-efficient when T is less than 31.
- Therefore, considering both energy consumption and accuracy, we recommend our SSF SNN with $T = 15$ as the optimal configuration for our ECG application.

This addresses Questions 1 and 4 from the introduction.

5.4 Patient-wise online training

Previously, we allocated 60% of the dataset for training and 20% for testing. Now, to further enhance accuracy and customize the model for individual patient needs, we train each patient's model using their specific 20% of heartbeats combined with the original 60% of training data, all based on pretrained weights learned from the entire training dataset with SNN of SSF ($T=15$). The remaining 20% serves as the test set for each patient. We display confusion matrices before and after this patient-specific online training. Additionally, we evaluate the performance before and after per-patient fine-tuning using two key metrics: sensitivity (Se) and positive predictivity (P+) [6], with calculations detailed below:

True Labels	0	1	2	3
0	17482	350	57	119
1	44	549	3	7
2	25	7	1327	28
3	14	0	8	138
	0	1	2	3
	Predicted Labels			

Fig. 7. Confusion matrix before patient-wise tuning

True Labels	0	1	2	3
0	17827	153	17	11
1	90	511	1	1
2	21	3	1356	7
3	21	0	20	119
	0	1	2	3
	Predicted Labels			

Fig. 8. Confusion matrix after patient-wise tuning

$$Se = \frac{TP}{TP + FN}; \quad (13)$$

$$P+ = \frac{TP}{TP + FP}. \quad (14)$$

where TP FN and FP indicate true positive, false negative and false positive.

As shown in Table 10, after fine-tuning, the classes N and VEB demonstrate improved performance in both sensitivity and positive predictivity. The overall accuracy of the SNN has increased by 1.57%. “8-bits sparrowSNN” and “8-bits sparrowSNN+” indicates the model before and after per-patient online training.

Table 9. SNN accuracy analysis.

	N		SVEB		VEB		F		Accuracy (%)
	Se	P+	Se	P+	Se	P+	Se	P+	
8-bits sparrowSNN	97.08	99.53	91.04	60.60	95.67	95.13	86.25	47.26	96.72
8-bits sparrowSNN+	98.99	99.26	84.74	76.61	97.76	97.27	74.38	86.23	98.29

5.5 Comparing the the state-of-the-art

In this work, we benchmark our designs against state-of-the-art (SOTA) models. Chu, *et. al.* [13] introduced a spike-driven SNN processor for always-on ECG classification, utilizing LC sampling for efficient temporal coding and event-driven processing. This is coupled with hardware-aware STBP training that achieves an SNN accuracy of 98.22% with an energy consumption of 0.75 μ J. This is 7.72% higher than the accuracy reported by Liu, *et. al.* [26]. Our ASIC design, which features a single compute unit (CU) and the hardware-friendly SSF spiking activation function, achieves even lower energy consumption at 0.031 μ J per inference, while maintaining a high detection accuracy of 98.29%. We also compare our results with other leading ANN models; for instance, Zhang, *et. al.* [50] achieves an accuracy of 96.69% with an energy consumption of 234.4nJ per inference. Here, we focus on comparing energy consumption rather than power due to differences in operating frequency across platforms.

Although existing baseline processors utilize various technology nodes, accurately estimating performance and energy differences relative to the process remains challenging. However, the substantial differences in magnitude suggest that sparrowSNN’s improved performance is not solely attributable to technology node differences.

Table 10. SNN accuracy analysis.

	OJCAS21 [14]	AS23 [50]	TCAS-II [10]	TBioCAS22 [29]	ISSCC22 [26]	TBioCAS22 [13]	This works
Process (nm)	40	55	180	28	180	40	22
Volatage (V)	0.6	1.2	1.8	0.57	1.2	1.1	0.8
Frequency (Hz)	70M	100K	5M	250k-5M	Asynchronous	65k-100M	4M
Areas (mm ²)	0.2123	0.33	0.75	0.54	10	0.3246	0.0409
Energy/inference	0.212 μ J	0.234 μ J	1.8 μ J	0.3 μ J	N/A	0.75 μ J	0.031 μ J
Methods	ELM	ANN	ANN	SNN	SNN	SNN	SNN
Accuracy (%)	92	96.69	98	98.6	90.5	98.22	98.29

6 DISCUSSIONS

6.1 Super low quantized ANNs vs SNNs

Pytorch-based post-training static quantization does not support low-bit activations, such as 3-bit or 4-bit, which can lead to significant accuracy reductions in an ASIC setting. To overcome this, we train our network using a clamp and quantization function (refer to Equation 4) instead of the standard ReLU activation. For instance, to quantize activations to 4 bits, the quantization level T should be set to 15. Algorithm 4 is then applied on the trained ANN M to perform weight and activation quantization. Initially, we determine the maximum and minimum values of both the weights and biases, f_{\max} and f_{\min} , to compute the scaling factor s_w for weight and bias quantization. We then run M on the entire training dataset to gather the scaling factors s_i for input activations and s_o for output activations, based on the layer’s maximum and minimum values across all training data. During quantized ANN inference, input data is scaled to its integer representation, multiplied by the integer weights, and added to the integer biases. Rescaling factors r_1 and r_2 map the integer output $x_{o,q}$ back to its original range.

To avoid multiplication for the rescaling factor or between integer weights and inputs, we quantize the rescaling factor to its nearest 2^{-I} , where I indicates the use of bit shifting for multiplication [33]. However, this approach can lead to significant accuracy loss due to the simplification of the rescaling factor. To mitigate this, we multiply the rescaling factor, such as r_1 , by a large number like 2^M and apply rounding. Subsequently, after multiplying by the adjusted rescaling factor, we perform an M -bit shift on the result to reduce information loss.

We achieved an SNN accuracy of 96.38% using an ANN with 8-bit weights and 4-bit activations. The calculations are similar, involving 4-bit to 8-bit integer multiplication. Additionally, our SNN includes a spike activation step, whereas the quantized ANN involves shifting and multiplying by a large integer. The core power consumption is similar for such ANN and SNN with SSF. The computational demand varies with the sparsity of the SNN. If sparsity is sufficiently high, the SNN with the SSF model becomes more energy-efficient than the quantized ANN. Conversely, in scenarios of low sparsity, a highly quantized ANN is more advantageous.

7 CONCLUSIONS

In this paper, we examine the energy consumption and accuracy impacts of spiking neural networks (SNNs) from a hardware perspective, focusing on aspects such as spike activation functions, network structures, and inference workflows using an ultra-low power wearable platform for ECG applications. We also present a fully co-designed software-hardware ASIC, sparrowSNN, for these platforms. On the MIT-BIH ECG dataset, sparrowSNN achieves a state-of-the-art accuracy of 98.29% with an energy consumption of only 31.39nJ. We believe our discussion

Algorithm 4 Low-bits ANN weight/bias/activations quantization for layer l

Require: Weight w^l of layer l ; Bias b^l of layer l ; Quantization level q that quantized weight/bias to q -bits integer;

Ensure: A well trained model M ; Input x_i and output x_o of layer l after running M on the training dataset.

1: **STEP1:** Go through the training dataset using M and collect:

2: $s_w = (\max\{w^l, b^l\} - \min\{w^l, b^l\}) / (2^q - 1)$

3: $w_q^l = \text{clamp}\{\lfloor (w^l/r) \rfloor, -2^{q-1}, 2^{q-1} - 1\}$

4: $b_q^l = \text{clamp}\{\lfloor (b^l/r) \rfloor, -2^{q-1}, 2^{q-1} - 1\}$

5: $s_i = (x_{i,\max} - x_{i,\min}) / (2^q - 1)$

6: $s_o = (x_{o,\max} - x_{o,\min}) / (2^q - 1)$

7:

8: **Step2:** Quantized inference

9: $x_{i,q} = \text{clamp}(\lfloor (x_i/s_i), 0, 2^q - 1 \rfloor)$

10: $r_1 = s_i * s_w / s_o$

11: $r_2 = s_w / s_o$

12: Mapping r_1, r_2 to nearest 2^{-I}

13: $x_{o,q} = \text{clamp}(\lfloor (w_q * x_{i,q} * r_1) \rfloor + \lfloor (b_q * r_2) \rfloor, 0, 2^q - 1)$

14: return $x_{o,q}$

and implementation of SNNs on hardware platforms will enhance understanding of their energy usage and operational workflows, contributing to advancements of the SNN on ultra-low wearable device.

REFERENCES

- [1] 2023. Pytorch Post Training Static Quantization. <https://pytorch.org/docs/stable/quantization.html>
- [2] 2024. Heart Disease Fact. <https://www.cdc.gov/heartdisease/facts.htm>
- [3] Raafat O Aburukba, Mazin AliKarrar, Taha Landolsi, and Khaled El-Fakih. 2020. Scheduling Internet of Things requests to minimize latency in hybrid Fog–Cloud computing. *Future Generation Computer Systems* 111 (2020), 539–551.
- [4] Adel A Ahmed, Waleed Ali, Talal AA Abdullah, and Sharaf J Malebary. 2023. Classifying cardiac arrhythmia from ECG signal using 1D CNN deep learning model. *Mathematics* 11, 3 (2023), 562.
- [5] Filipp Akopyan, Jun Sawada, Andrew Cassidy, Rodrigo Alvarez-Icaza, John Arthur, Paul Merolla, Nabil Imam, Yutaka Nakamura, Pallab Datta, Gi-Joon Nam, et al. 2015. Truenorth: Design and tool flow of a 65 mw 1 million neuron programmable neurosynaptic chip. *IEEE transactions on computer-aided design of integrated circuits and systems* 34, 10 (2015), 1537–1557.
- [6] Douglas G Altman and J Martin Bland. 1994. Statistics Notes: Diagnostic tests 2: predictive values. *Bmj* 309, 6947 (1994), 102.
- [7] Dimitra Azariadi, Vasileios Tsoutsouras, Sotirios Xydis, and Dimitrios Soudris. 2016. ECG signal analysis and arrhythmia detection on IoT wearable medical devices. In *2016 5th International conference on modern circuits and systems technologies (MOCASST)*. IEEE, 1–4.
- [8] Abhiroop Bhattacharjee, Ruokai Yin, Abhishek Moitra, and Priyadarshini Panda. 2024. Are SNNs Truly Energy-efficient?—A Hardware Perspective. In *ICASSP 2024-2024 IEEE International Conference on Acoustics, Speech and Signal Processing (ICASSP)*. IEEE, 13311–13315.
- [9] Romain Brette. 2015. Philosophy of the spike: rate-based vs. spike-based theories of the brain. *Frontiers in systems neuroscience* 9 (2015), 151.
- [10] Qiao Cai, Xinzi Xu, Yang Zhao, Liang Ying, Yongfu Li, and Yong Lian. 2021. A 1.3 μ W event-driven ANN core for cardiac arrhythmia classification in wearable sensors. *IEEE Transactions on Circuits and Systems II: Express Briefs* 68, 9 (2021), 3123–3127.
- [11] Nitesh V Chawla, Kevin W Bowyer, Lawrence O Hall, and W Philip Kegelmeyer. 2002. SMOTE: synthetic minority over-sampling technique. *Journal of artificial intelligence research* 16 (2002), 321–357.
- [12] Shichao Chen, Qijie Li, Mengchu Zhou, and Abdullah Abusorrah. 2021. Recent advances in collaborative scheduling of computing tasks in an edge computing paradigm. *Sensors* 21, 3 (2021), 779.
- [13] Haoming Chu, Yulong Yan, Leijing Gan, Hao Jia, Liyu Qian, Yuxiang Huan, Lirong Zheng, and Zhuo Zou. 2022. A neuromorphic processing system with spike-driven SNN processor for wearable ECG classification. *IEEE Transactions on Biomedical Circuits and Systems* 16, 4 (2022), 511–523.
- [14] Yu-Chuan Chuang, Yi-Ta Chen, Huai-Ting Li, and An-Yeu Andy Wu. 2021. An arbitrarily reconfigurable extreme learning machine inference engine for robust ECG anomaly detection. *IEEE Open Journal of Circuits and Systems* 2 (2021), 196–209.
- [15] Philip De Chazal, Maria O’Dwyer, and Richard B Reilly. 2004. Automatic classification of heartbeats using ECG morphology and heartbeat interval features. *IEEE transactions on biomedical engineering* 51, 7 (2004), 1196–1206.
- [16] Diego di Bernardo and Alan Murray. 2000. Explaining the T-wave shape in the ECG. *Nature* 403, 6765 (2000), 40–40.
- [17] Peter U Diehl, Daniel Neil, Jonathan Binas, Matthew Cook, Shih-Chii Liu, and Michael Pfeiffer. 2015. Fast-classifying, high-accuracy spiking deep networks through weight and threshold balancing. In *2015 International Joint Conference on Neural Networks (IJCNN)*. IEEE, 1–8.
- [18] Jason K Eshraghian, Max Ward, Emre O Neftci, Xinxin Wang, Gregor Lenz, Girish Dwivedi, Mohammed Bennamoun, Doo Seok Jeong, and Wei D Lu. 2023. Training spiking neural networks using lessons from deep learning. *Proc. IEEE* (2023).
- [19] Yifei Feng, Shijia Geng, Jianjun Chu, Zhaoji Fu, and Shenda Hong. 2022. Building and training a deep spiking neural network for ECG classification. *Biomedical Signal Processing and Control* 77 (2022), 103749.
- [20] Association for the Advancement of Medical Instrumentation et al. 1998. Testing and reporting performance results of cardiac rhythm and ST segment measurement algorithms. *ANSI/AAMI EC38* 1998 (1998).
- [21] Chittotosh Ganguly and Saswat Chakrabarti. 2020. A discrete time framework for spike transfer process in a cortical neuron with asynchronous epsp, ipsp, and variable threshold. *IEEE Transactions on Neural Systems and Rehabilitation Engineering* 28, 4 (2020), 772–781.
- [22] V Jahmunah, Shu Lih Oh, Joel Koh En Wei, Edward J Ciaccio, Kuang Chua, Tan Ru San, and U Rajendra Acharya. 2019. Computer-aided diagnosis of congestive heart failure using ECG signals—A review. *Physica Medica* 62 (2019), 95–104.
- [23] Congfeng Jiang, Tiantian Fan, Honghao Gao, Weisong Shi, Liangkai Liu, Christophe Cérin, and Jian Wan. 2020. Energy aware edge computing: A survey. *Computer Communications* 151 (2020), 556–580.
- [24] Yubin Kim, Xuhai Xu, Daniel McDuff, Cynthia Breazeal, and Hae Won Park. 2024. Health-llm: Large language models for health prediction via wearable sensor data. *arXiv preprint arXiv:2401.06866* (2024).
- [25] Yanzhen Liu, Zhijin Qin, and Geoffrey Ye Li. 2024. Energy-Efficient Distributed Spiking Neural Network for Wireless Edge Intelligence. *IEEE Transactions on Wireless Communications* (2024).
- [26] Ying Liu, Zhixuan Wang, Wei He, Linxiao Shen, Yihan Zhang, Peiyu Chen, Meng Wu, Hao Zhang, Peng Zhou, Jinguang Liu, et al. 2022. An 82nW 0.53 pJ/SOP clock-free spiking neural network with 40 μ s latency for AIoT wake-up functions using ultimate-event-driven bionic architecture and computing-in-memory technique. In *2022 IEEE International Solid-State Circuits Conference (ISSCC)*, Vol. 65. IEEE,

- 372–374.
- [27] Eduardo José da S Luz, William Robson Schwartz, Guillermo Cámara-Chávez, and David Menotti. 2016. ECG-based heartbeat classification for arrhythmia detection: A survey. *Computer methods and programs in biomedicine* 127 (2016), 144–164.
- [28] Sumit Majumder, Emad Aghayi, Moein Noferesti, Hamidreza Memarzadeh-Tehran, Tapas Mondal, Zhibo Pang, and M Jamal Deen. 2017. Smart homes for elderly healthcare—Recent advances and research challenges. *Sensors* 17, 11 (2017), 2496.
- [29] Ruixin Mao, Sixu Li, Zhaomin Zhang, Zihan Xia, Jianbiao Xiao, Zixuan Zhu, Jiahao Liu, Weiwei Shan, Liang Chang, and Jun Zhou. 2022. An ultra-energy-efficient and high accuracy ECG classification processor with SNN inference assisted by on-chip ANN learning. *IEEE Transactions on Biomedical Circuits and Systems* 16, 5 (2022), 832–841.
- [30] Tanis Mar, Sebastian Zauneder, Juan Pablo Martínez, Mariano Llamedo, and Rüdiger Poll. 2011. Optimization of ECG classification by means of feature selection. *IEEE transactions on Biomedical Engineering* 58, 8 (2011), 2168–2177.
- [31] Abhishek Moitra, Abhiroop Bhattacharjee, Runcong Kuang, Gokul Krishnan, Yu Cao, and Priyadarshini Panda. 2023. Spikesim: An end-to-end compute-in-memory hardware evaluation tool for benchmarking spiking neural networks. *IEEE Transactions on Computer-Aided Design of Integrated Circuits and Systems* (2023).
- [32] George B Moody and Roger G Mark. 2001. The impact of the MIT-BIH arrhythmia database. *IEEE Engineering in Medicine and Biology Magazine* 20, 3 (2001), 45–50.
- [33] Markus Nagel, Marios Fournarakis, Rana Ali Amjad, Yelysei Bondarenko, Mart Van Baalen, and Tijmen Blankevoort. 2021. A white paper on neural network quantization. *arXiv preprint arXiv:2106.08295* (2021).
- [34] Nafiul Rashid, Manik Dautta, Peter Tseng, and Mohammad Abdullah Al Faruque. 2020. HEAR: Fog-enabled energy-aware online human eating activity recognition. *IEEE Internet of Things Journal* 8, 2 (2020), 860–868.
- [35] Nafiul Rashid, Berken Utku Demirel, Mohanad Odema, and Mohammad Abdullah Al Faruque. 2022. Template matching based early exit cnn for energy-efficient myocardial infarction detection on low-power wearable devices. *Proceedings of the ACM on Interactive, Mobile, Wearable and Ubiquitous Technologies* 6, 2 (2022), 1–22.
- [36] Bodo Rueckauer, Iulia-Alexandra Lungu, Yuhuang Hu, Michael Pfeiffer, and Shih-Chii Liu. 2017. Conversion of continuous-valued deep networks to efficient event-driven networks for image classification. *Frontiers in Neuroscience* 11 (2017), 682.
- [37] Richard B Stein, E Roderich Gossen, and Kelvin E Jones. 2005. Neuronal variability: noise or part of the signal? *Nature Reviews Neuroscience* 6, 5 (2005), 389–397.
- [38] Aboozar Taherkhani, Ammar Belatreche, Yuhua Li, Georgina Cosma, Liam Maguire, and T.M. McGinnity. 2019. A review of learning in biologically plausible spiking neural networks. *Neural Networks* 122 (10 2019). <https://doi.org/10.1016/j.neunet.2019.09.036>
- [39] Chengcheng Tang and Jie Han. 2023. Hardware efficient weight-binarized spiking neural networks. In *2023 Design, Automation & Test in Europe Conference & Exhibition (DATE)*. IEEE, 1–6.
- [40] Amina Tihak, Lejla Smajlovic, and Dusanka Boskovic. 2023. Classification of Atrial Fibrillation ECG Signals Using 2D CNN. In *Mediterranean Conference on Medical and Biological Engineering and Computing*. Springer, 57–65.
- [41] Alex Vigneron and Jean Martinet. 2020. A critical survey of STDP in Spiking Neural Networks for Pattern Recognition (Preprint). (03 2020). <https://doi.org/10.13140/RG.2.2.24086.09287>
- [42] K Vinutha and Usharani Thirunavukkarasu. 2023. Prediction of arrhythmia from MIT-BIH database using random forest (RF) and voted perceptron (VP) classifiers. In *AIP Conference Proceedings*, Vol. 2822. AIP Publishing.
- [43] Ning Wang, Jun Zhou, Guanghai Dai, Jiahui Huang, and Yuxiang Xie. 2019. Energy-efficient intelligent ECG monitoring for wearable devices. *IEEE transactions on biomedical circuits and systems* 13, 5 (2019), 1112–1121.
- [44] Xiyuan Wu, Yufei Zhao, Yong Song, Yurong Jiang, Yashuo Bai, Xinyi Li, Ya Zhou, Xin Yang, and Qun Hao. 2023. Dynamic threshold integrate and fire neuron model for low latency spiking neural networks. *Neurocomputing* 544 (2023), 126247.
- [45] Yujie Wu, Lei Deng, Guoqi Li, Jun Zhu, Yuan Xie, and Luping Shi. 2019. Direct training for spiking neural networks: Faster, larger, better. In *Proceedings of the AAAI Conference on Artificial Intelligence*, Vol. 33. 1311–1318.
- [46] Yulong Yan, Haoming Chu, Yi Jin, Yuxiang Huan, Zhuo Zou, and Lirong Zheng. 2022. Backpropagation with sparsity regularization for spiking neural network learning. *Frontiers in Neuroscience* 16 (2022), 760298.
- [47] Zhanglu Yan, Jun Zhou, and Weng-Fai Wong. 2021. Energy efficient ECG classification with spiking neural network. *Biomedical Signal Processing and Control* 63 (2021), 102170.
- [48] Zhanglu Yan, Jun Zhou, and Weng-Fai Wong. 2021. Near lossless transfer learning for spiking neural networks. In *Proceedings of the AAAI conference on artificial intelligence*, Vol. 35. 10577–10584.
- [49] Zhanglu Yan, Jun Zhou, and Weng-Fai Wong. 2023. CQ⁺ Training: Minimizing Accuracy Loss in Conversion from Convolutional Neural Networks to Spiking Neural Networks. *IEEE Transactions on Pattern Analysis and Machine Intelligence* (2023), 1–12. <https://doi.org/10.1109/TPAMI.2023.3286121>
- [50] Chen Zhang, Junfeng Chang, Yujiang Guan, Qiuping Li, Xin’an Wang, and Xing Zhang. 2023. A Low-Power ECG Processor ASIC Based on an Artificial Neural Network for Arrhythmia Detection. *Applied Sciences* 13, 17 (2023), 9591.
- [51] Yuxuan Zhao, Jiadong Ren, Bing Zhang, Jinxiao Wu, and Yongqiang Lyu. 2023. An explainable attention-based TCN heartbeats classification model for arrhythmia detection. *Biomedical Signal Processing and Control* 80 (2023), 104337.

Received 20 February 2007; revised 12 March 2009; accepted 5 June 2009